Available online at www.sciencedirect.com
SCIENCE DIRECT®
Polymer 45 (2004) 881–891
polymer
www.elsevier.com/locate/polymer

Flame retardant mechanism of polyamide 6–clay nanocomposites☆

Takashi Kashiwagi[a,*], Richard H. Harris Jr[a], Xin Zhang[b], R.M. Briber[b], Bani H. Cipriano[c], Srinivasa R. Raghavan[c], Walid H. Awad[a], John R. Shields[a]

[a]*Fire Science Division, Building and Fire Research Laboratory NIST, Gaithersburg, MD 20899-8665, USA*
[b]*Department of Materials Science and Engineering, University of Maryland, College Park, MD 20742, USA*
[c]*Department of Chemical Engineering, University of Maryland, College Park, MD 20742, USA*

Received 21 July 2003; received in revised form 14 November 2003; accepted 18 November 2003

Abstract

The thermal and flammability properties of polyamide 6/clay (2 and 5% by mass fraction) nanocomposites were measured to determine their flame retardant (FR) performance. The gasification process of the nanocomposite samples at an external radiant flux of 50 kW/m^2 in a nitrogen atmosphere was observed, and the residues collected at various sample mass losses were analyzed by thermogravimetric analysis, transmission electron microscopy, and X-ray diffraction to determine the content of the residue and to understand the FR mechanism of the nanocomposites. The analysis of the floccules of blackened residues shows that up to 80% by mass of the residues consists of clay particles and the remainder is thermally stable organic components with possible graphitic structure. Furthermore, clay particles are stacked in the carbonaceous floccule residues and the d-spacing of the clay platelets is in the range of 1.3–1.4 nm as compared to the well exfoliated original sample. The accumulation of the initially well-dispersed clay particles in the sample on the burning/gasifying sample surface are due to two possible mechanisms. One is recession of the polymer resin from the surface by pyrolysis with the de-wetted clay particles left behind. Another mechanism is the transportation of clay particles pushed by numerous rising bubbles of degradation products and the associated convection flow in the melt from the interior of the sample toward the sample surface. Numerous rising bubbles may have another effect on the transport of clay particles. Bursting of the bubbles at the sample surface pushes the accumulated clay particles outward from the bursting area and forms the island-like floccules instead of forming a continuous net-like structure of a clay filled protective layer. Therefore, both PA6/clay nanocomposite samples did not produce sufficient amounts of protective floccules to cover the entire sample surface and vigorous bubbling was observed over the sample surface which was not covered by the protective floccules.

Keywords: Flammability; Polyamide 6–clay nanocomposite; Flame retardant

1. Introduction

Polymer–clay nanocomposites have attracted a great deal of interest due to their improved mechanical, thermal and biodegradability properties [1–6]. Furthermore, an improvement in the flammability properties of polymers has been achieved with polymer–clay nanocomposites, which could provide an alternative to conventional flame retardants (FR) [7–15]. Several mechanisms have been proposed to describe the observed improvement in flammability properties of polymers by the formation of polymer–clay nanocomposites. One of them is the reduction in heat release rate due to the formation of a protective surface barrier/insulation layer consisting of accumulated clay platelets with a small amount of carbonaceous char [8,11]. Another mechanism proposed by Wilkie et al. is radical trapping by paramagnetic iron within the clay [12]. They showed that even when the clay was as low as 0.1% by mass fraction, the peak heat release rate of the clay/polystyrene nanocomposite was lowered by 40%, a value not much different from that observed with higher amounts of clay.

In our recent study of a silica based polymer nanocomposite, it was observed that the accumulated amount of silica particles on the sample surface, and their coverage over the exposed sample surface during burning, have a significant effect on the reduction of heat release rate of poly(methyl methacrylate) [16]. Both the accumulation and the surface coverage are affected by melt flow and by the

☆ This article is a US Government work and, as such, is in the public domain in the United States of America

* Corresponding author. Tel.: +1-301-975-6699; fax: +1-301-975-4052.
E-mail address: takashi.kashiwagi@nist.gov (T. Kashiwagi).

0032-3861/$ - see front matter © 2003 Elsevier Ltd. All rights reserved.
doi:10.1016/j.polymer.2003.11.036

bubbling of evolved degradation products near the sample surface. Therefore, it is important to understand the fate of clay particles in the molten layer near the sample surface to see if this sheds light on the FR mechanism. The key question is where are the initially well-dispersed clay particles during burning? The accumulation of clay particles near the sample surface and their area coverage over the degrading sample surface could be critical factors in determining their FR effectiveness.

In this study, the accumulation of clay particles and their coverage over the sample surface were measured by video images. Thermal gravimetric analyses and X-ray diffraction (XRD) measurement were conducted on residues collected at various times with samples having lost different fractions of the initial sample mass during the gasification experiment. The FR mechanism of the polymer–clay nanocomposite is explained on the basis of the above described results and other measurements of melt viscosity and of clay characteristics in the collected residues.

2. Experiment

2.1. Materials and sample preparation

Polyamide 6 (PA6) was selected as a resin for this study and commercially available PA6/clay samples were used. They were PA6 homopolymer (molecular mass (M_w) of about 15,000 g/mol, UBE 1015B[1]), PA6 ($M_w \approx 15,000$) with montmorillonite (MMT) of 2% by mass fraction (UBE 1015C2), and PA6 ($M_w \approx 18,000$) with MMT of 5% by mass fraction (UBE 1018C5). They were selected due to their exfoliated clay dispersion in PA6. Sample disks for the cone calorimeter, gasification, and rheology experiments were prepared using an injection molding machine (Gluco LP20B). All pellet samples were dried for 2 h at 75 °C, and kept in a desiccator over a desiccant until they were added to the injection molding machine. All samples were molded at 280 °C. The disks were 75 mm diameter with a thickness of 8 mm. No additional drying of the disk samples was made.

2.2. Transmission electron microscopy (TEM)

One block of injection molded sample was cut from the sample disk and cryotomed on a Leica Ultramicrotome with a Mircostar diamond knife. Cutting temperature was −70 °C. Section thickness was about 100 nm. TEM samples were obtained from the clay-char layer, the partial carbonized portion and the uncarbonized portion of the sample. These parts of the sample were embedded in Spurr epoxy resin and microtomed with an American Optical ULTRACUT microtome at room temperature. The thickness of the sections was estimated to be about 60 nm. Thin sections were observed in a Hitachi 600 transmission electron microscope at 100 kV. The TEM negatives were scanned with an EPSON scanner at 2400 DPI.

2.3. X-ray diffraction

The XRD data were collected on powder specimens with a Philips diffractometer using Cu Kα radiation ($\lambda = 0.154$ nm) with a 0.04° 2θ step size and a 3 s count time per step.

2.4. Rheology

Although several studies of the rheological properties of polyamides/clay nanocomposites have been previously published, they were limited to the range of relatively low temperatures (up to processing temperatures) [17,18]. In this study, experiments were conducted in a nitrogen atmosphere over a temperature range which is close to the degradation temperature of the sample. Dynamic rheological experiments were performed on a Rheometrics RDA-3 rheometer using a 25 mm parallel plate geometry. Samples used for rheological experiments were disks of 25 mm diameter and ca. 1 mm thickness cut from the injection-molded disks described earlier. Prior to measurement, the samples were dried in a vacuum oven at 120 °C for a period of 24 h [17]. Rheological experiments were conducted in an inert nitrogen atmosphere over a temperature range between 235 and 350 °C. Temperature ramp tests spanning this range were performed at a heating rate of 2 °C/min with the frequency held constant at 5 s^{-1} and the strain amplitude at 10%. This strain amplitude was ascertained to be within the linear viscoelastic region of all the samples. Care was also taken to ensure that the normal force measured by the instrument was negligible prior to beginning each rheological experiment.

2.5. Thermal stability and flammability property measurement

Thermogravimetric analysis (TGA) was conducted using a TA Instruments 2950. The samples were tested under N_2 from 30 to 800 °C at a heating rate of 10 °C/min. The standard uncertainty on sample mass measurement was ±1%. The flammability properties including heat release rate were measured with a cone calorimeter at an incident heat flux of 50 kW/m^2 in accord with ASTM E 1356. The standard uncertainty of the measured heat release rate was ±10% [7]. All tests were run in the horizontal orientation.

A radiant gasification apparatus, somewhat similar to a cone calorimeter, was designed and constructed at NIST to study the gasification processes of samples by measuring mass loss rate and temperatures of the sample exposed to a fire like heat flux in a nitrogen atmosphere (no burning). All

[1] Certain commercial equipment, instruments, materials, services or companies are identified in this article to specify adequately the experimental procedure. This in no way implies endorsement or recommendation by the National Institutes of Standards and Technology (NIST).

experiments were conducted at 50 kW/m^2. The unique nature of this device is threefold: (1) observation and results obtained from it are only based on the condensed phase processes due to the absence of any gas phase oxidation reactions and processes; (2) it enables visual observations of gasification behavior of a sample using a video camera under a radiant flux similar to that of a fire without any interference from a flame; (3) the external flux to the sample surface is well-defined and nearly constant over the duration of an entire experiment (and over the spatial extent of the sample surface) due to the absence of heat feedback from a flame. A more detailed discussion of the apparatus is given in our previous study [19]; the standard uncertainty of the measured mass loss was within 10%.

3. Results

3.1. Thermal stability

Normalized sample mass loss rate in percentage divided by the heating rate is plotted versus temperature in Fig. 1 for each of the three samples of PA6, PA6/clay(2%), and PA6/clay(5%). The results show one large peak in the mass loss rate for each of the three samples and the thermal stability of the nanocomposites does not vary significantly from that of the PA6 sample, except for a small, earlier mass loss starting at about 350 °C for the PA6/clay(5%) sample compared to the other two samples. This loss could be caused by the thermal degradation of the organic treatment on the clay surface (the total amount of the organic surface treatment component is about mass fraction of 0.6%, and 1.5% in the 2% and 5% nanocomposite samples, respectively.) [20].

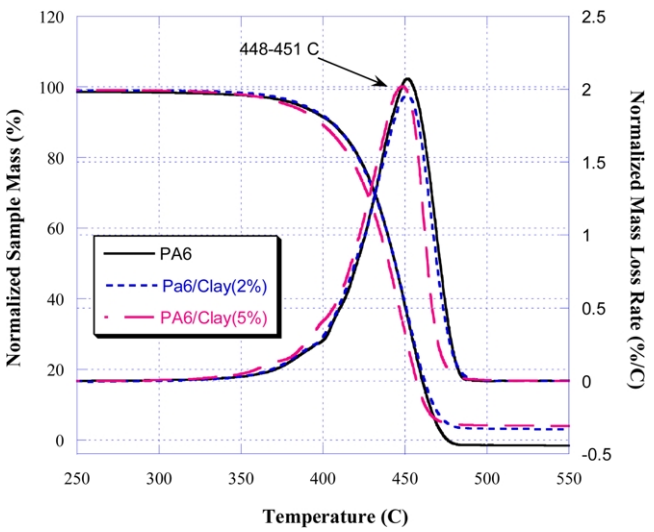

Fig. 1. Normalized sample mass and mass loss rate curves in N2 at 10 °C/min.

3.2. Rheology

Fig. 2 shows the complex viscosity η^* as a function of temperature for the PA6 melt and for the nanocomposites with 2% clay (PA6-C2) and 5% clay (PA6-C5). The viscosity η^* is practically identical for the neat polymer and for the 2% nanocomposite. However, the 5% nanocomposite shows a significantly higher viscosity, especially at low temperatures (ca. 250 °C). A further examination of the contributions to the complex viscosity η^* from the elastic modulus (G') and the viscous modulus (G'') reveals the differences in microstructure between the samples. The trends in viscous modulus G'' practically mirror the trends in η^* over the entire temperature range, indicating its dominant contribution to η^* at this frequency. The 5% nanocomposite shows a significant elastic modulus, especially at low temperatures. Indeed, frequency sweep data (not shown) reveal that G' dominates over G'' at long timescales (very low frequencies), with both moduli being practically independent of frequency. This suggests that there exists a sample-spanning network structure composed of clay particles and polymer chains in the 5% nanocomposite.

3.3. Flammability properties

Heat release rate curves of the three samples are shown in Fig. 3. The results show that the nanocomposite samples slightly increase the ignition delay time and significantly reduce the peak heat release rate in comparison to pristine PA6. The greater the clay content the lower the heat release rate. The calculated total heat release per unit surface area (integrated over time = area of the curve) is 28 ± 1 MJ/m^2 for PA6, 27 ± 1 MJ/m^2 for PA6/clay(2%), and 26 ± 1 MJ/m^2 for PA6/clay(5%). There is no significant reduction in total heat release due to the nanocomposites for the level of clay contents used in this study. This indicates that the

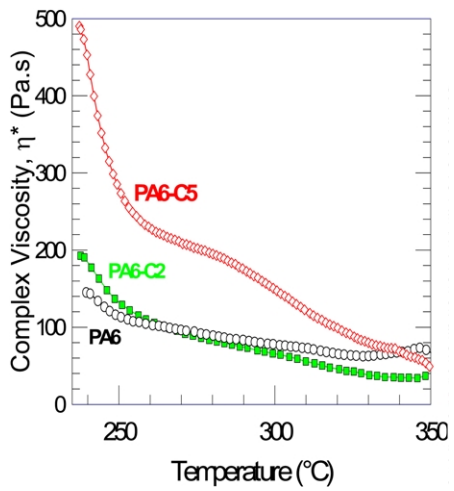

Fig. 2. Complex viscosity vs temperature for the three samples at a heating rate of 2 °C/min with the frequency at 5 s^{-1} in nitrogen.

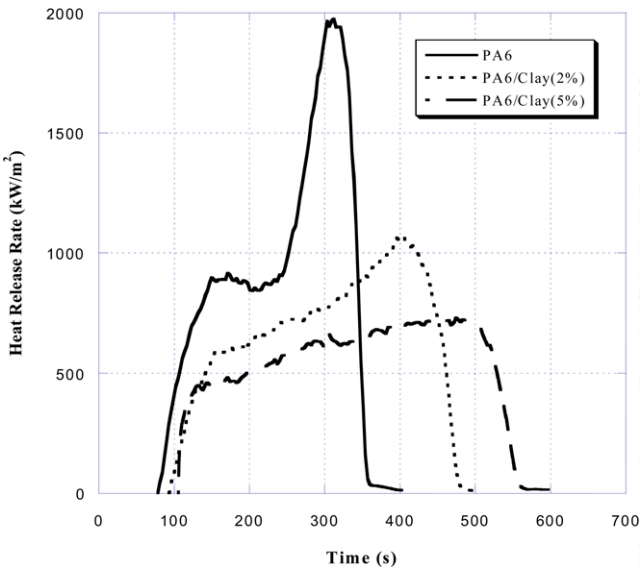

Fig. 3. Effects of clay content on heat release rate of PA6 (8 mm thick) at 50 kW/m^2.

nanocomposites burn slowly but they burn nearly completely. Slow burning of the composites can be seen from the mass loss (burning) rate curves shown in Fig. 4. The mass loss rate curve of each sample is proportional to the heat release rate curve. Thus, the specific heat of combustion obtained from the heat release rate divided by mass loss rate is 30 ± 2 kJ/g for the three samples. This unchanged specific heat of combustion implies that the observed reduction in heat release rate (and mass burning rate) tends to be due to chemical and physical processes mainly in the condensed phase instead of in the gas phase. In order to prove this conjecture, the samples were exposed to the same external flux as that in the cone calorimeter but in a nitrogen atmosphere to avoid any gas phase effects.

3.4. Gasification in a nitrogen atmosphere

The radiation-forced mass loss rate curve of each of the three samples is shown in Fig. 5. These curves are quite reproducible in repeated tests. A comparison between the results shown in Fig. 4 and those shown in Fig. 5 indicates that the mass burning rate for each sample is higher than the corresponding forced gasification rate; the mass burning rate curves also shift toward earlier time than the gasification rate curves as a result. In the burning case, two different fluxes are supplied to the sample surface; one is an external radiant flux and the other is the heat feedback from the flame. However, in the gasification case, only the former is supplied to the sample surface. Therefore, the additional heat feedback from the flame generates a higher mass burning rate (which produces a larger flame and higher heat feedback to the sample surface) and a shift toward earlier time of the mass burning rate curves than the gasification rate curves. This is the reason why the reduction in the mass burning rate by the nanocomposites is larger than the reduction in the mass loss rate in the forced gasification case. Although there is a quantitative difference in mass loss rate between the two cases, the overall differences among the three samples are very similar between the burning case and the gasification case. The burning process depends on the chemical and physical processes in both the gas phase and the condensed phase, but the gasification process depends only on those in the

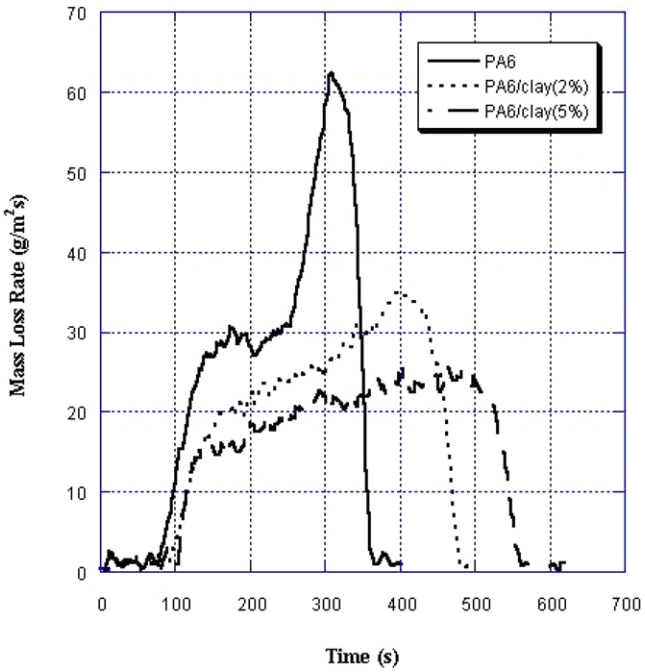

Fig. 4. Effects of clay content on mass burning rate of PA6 (8 mm thick) at 50 kW/m^2.

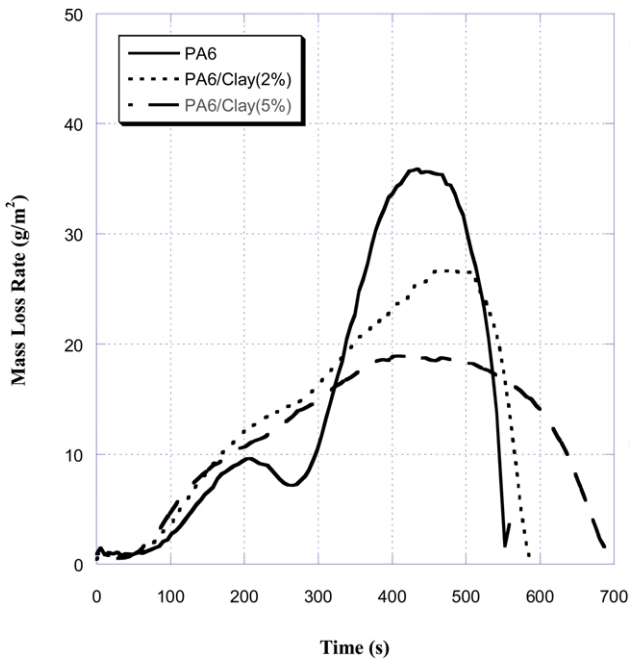

Fig. 5. Effects of clay content on mass loss rate of PA6 (8 mm thick) in N_2 at 50 kW/m^2.

condensed phase. This indicates that the observed improvement in the flammability property of the nanocomposites is mainly due to the chemical and physical processes in the condensed phase.

Observation of the sequence of events in the non-flaming gasification of the PA6 sample without clay first revealed small bubbles of evolved degradation products at the sample surface, followed by the appearance of many large bubbles. About 60 s after the start of irradiation, the size of the bubbles became gradually smaller and around 120 s many small bubbles with few larger size bubbles appeared, as shown in Fig. 6. The sample appeared less viscous (fluid-like) with numerous small bubbles. Shortly after 200 s, some swelling of the sample was observed giving it the appearance of a highly viscous mound. This effect could have been caused by lifting of the solid sample below the fluid like layer by downward flow of molten polymer along the perimeter of the sample container. There appear to be sample size effects on mass loss rate. This feature might be the reason why there is a dip in the mass loss rate curve around 260 s. This dip was quite reproducible in repeated tests. Furthermore, a similar trend can be seen in the heat release rate and burning mass loss rate curves as shown in Figs. 3 and 4. Vigorous bubbling in the very fluid-like upper layer of the sample continued, and the sample surface gradually darkened after 400 s. A very thin, black coating over the bottom of the container was left at the end of the test. The amount of the residue at the end of the test was less than 1% of the initial sample mass.

The gasification behavior of the PA6/clay(2%) sample was initially similar to that of the PA6 sample except that it appeared to be more viscous; it still had the appearance of a viscous fluid. Around 150 s several small, dark floccules appeared on the surface and these grew with time, as shown in Fig. 6. However, they never covered the entire sample surface. Numerous small dark floccules were formed together with few large floccules. The dark crust-like floccules were left at the bottom of the container at the end of the test. The mass of the residue was about 2% of the initial sample mass. The PA6/clay(5%) appeared to be much more viscous than the PA6 sample during the gasification test but it still formed numerous larger bubbles. Around 100 s after the start of irradiation, a thin, black ring (not continuously connected) appeared at the perimeter of the sample and this ring moved toward the center of the sample then collapsed to form a large black clump around 150 s. More carbonaceous floccules appeared near the perimeter of the sample and moved gradually toward the center and formed larger rough-surface floccules. This can be seen in the images at 200 s in Fig. 6. Vigorous bubbling of evolved

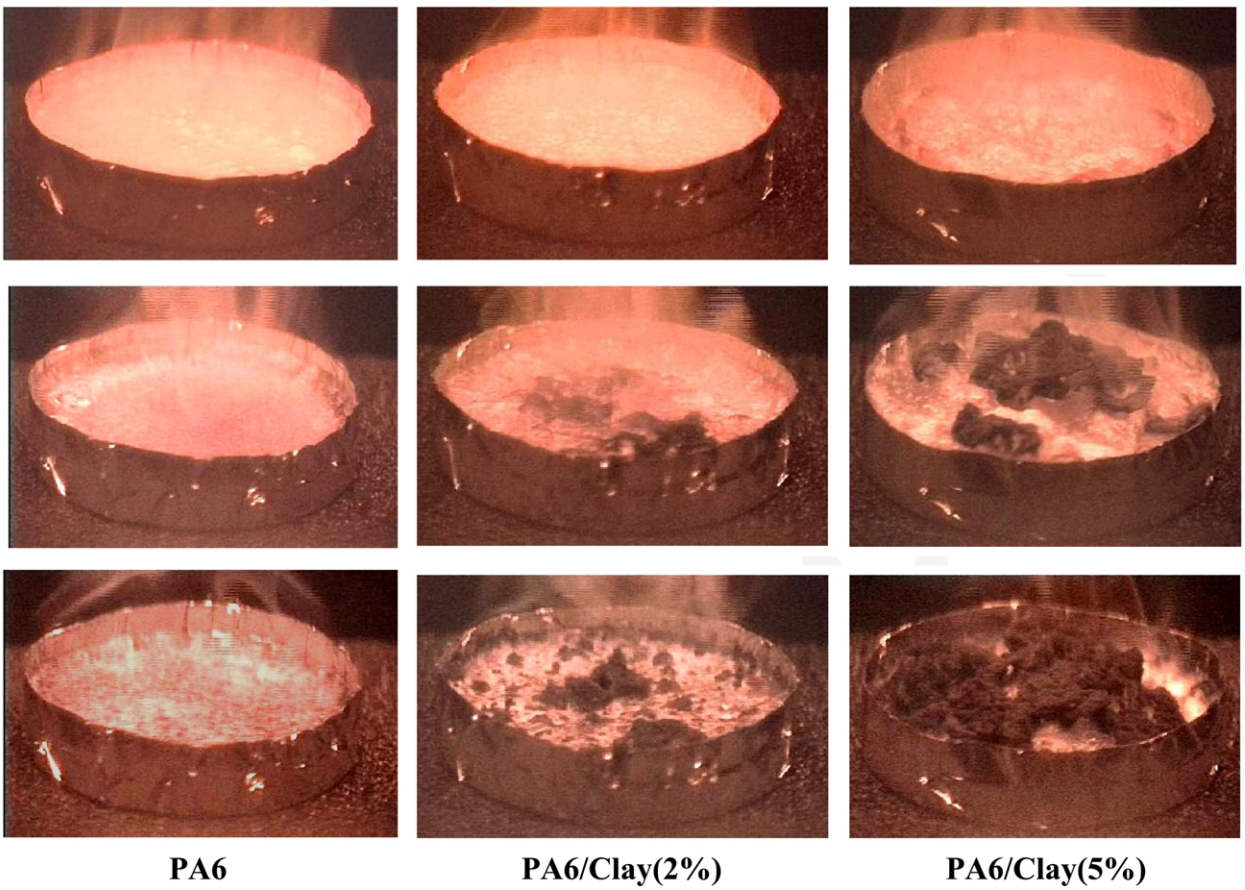

Fig. 6. Selected video images at 100, 200, and 400 s in nitrogen at 50 kW/m^2.

degradation products was observed over that portion of the sample surface which was not covered by the carbonaceous floccules. The floccules gradually grew and were left at the bottom of the container at the end of the test. The mass of the residue was about 5% of the initial sample mass. A picture of the residue collected after the test is shown for each sample in Fig. 7. These residues look like char and are brittle and fragile. The PA6/clay(5%) generated more residue of the carbonaceous floccules than the PA6/clay(2%) sample. Similar carbonaceous floccules were also observed in the residues of the burned samples tested in the cone calorimeter. These pictures indicate that the formation of the protective, carbonaceous floccules and their coverage over the sample surface are desirable as a means of reducing the exposure of the molten polymer to external radiant flux or to heat feedback from flame. For most effective FR performance, they need to cover the entire sample surface in order to fully shield/protect the polymer melt.

3.5. Characterization of the collected residues

It is important to determine the composition of the carbonaceous floccules. Vigorous bubbling was observed over the sample surface not covered by the protective floccules, as described above. It is quite possible to transport clay particles through the molten layer in the flow motion generated by the rising bubbles. Since the clay particles (without the organic surface treatment) should stay in the residue at the end of the gasification test, they should be accumulated in the protective floccules which are the only residue shown in Fig. 7. In order to confirm this, samples of these protective floccules were collected after PA6/clay(5%) had lost several differing fractions of initial mass in the gasification experiment. Pictures of the collected residue are shown in Fig. 8. They indicate the growth of the carbonaceous floccules covering more surface area as the experiment progressed. However, they did not cover the entire sample surface and the pictures show white uncovered regions where vigorous bubbling was observed during the tests, as shown in Fig. 6. Small samples of the black, protective floccules and of the white regions were collected for further analysis. TGA analysis of the carbonaceous floccules was conducted in air at a heating rate of 10 °C/m up to 800 °C and the results are shown in Fig. 9. A light gray residue was observed at the end of the TGA test. The residue is assumed to be clay without any organics. The results show a rapid increase of clay content in the floccules up to about mass fraction of 80%, by the point at which the irradiated sample had lost only about 20% by mass. After about 20% sample mass loss, the clay content in the carbonaceous floccules does not significantly increase.

The derivative of normalized sample mass loss with respective to temperature (DTG), using the results shown in Fig. 9, was taken and the results are shown in Fig. 10. The original PA6/clay(5%) sample shows a sharp peak around 430 °C followed by a small, broad peak around 550 °C. Since the carbonaceous floccule residues collected at the sample mass losses of 10 and 17% contain a relatively small amount of clay particles (up to about 30% by mass), they contain more organics; their DTG data show the same sharp peak as that of the original sample with additional small peaks at around 330, 560, and 720 °C. For the carbonaceous floccule residues collected at higher sample mass losses, their DTG curves show small peaks at around 600 and 720 °C. These results indicate that the carbonaceous floccule residues collected at the sample mass losses of up to about 20% by mass contain the PA6 structure but lose it with higher sample mass losses. The organic content in the carbonaceous floccule residues above 20% sample mass losses is more thermally stable than PA6 and its structure might be aromatic nature.

The accumulation of clay particles in the carbonaceous floccule residues raises the question of the structure of the clay particles in them. TEM images of the original sample and those of the residue collected at 17% sample mass loss were compared to examine the difference in the clay structure. In the original sample, the clay platelets are fully exfoliated as shown in Fig. 11. Note at the position labeled

Fig. 7. Residue pictures at the end of the gasification tests in N_2 at 50 kW/m^2.

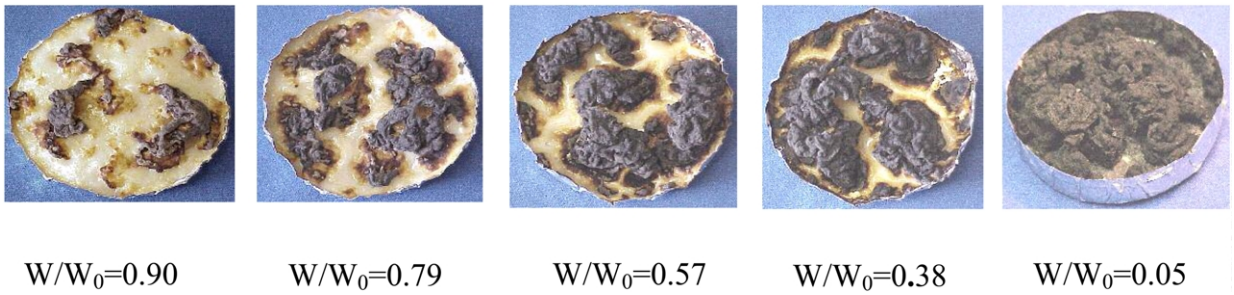

Fig. 8. Pictures of the residues of PA6/Clay(5%) collected when it lost various fractions of its mass in a nitrogen atmosphere at 50 kW/m^2.

'A' in the figure, two platelets spaced approximately 1.5 nm apart can be seen clearly. However, such close platelets are rare. Large groups of wavy clay platelets are found in the carbonaceous floccule residues, as shown in Fig. 12. The platelets are much closer to each other than those in the original sample. Wide-angle XRD measurements were conducted for the collected carbonaceous floccule residues to obtain clay particle structure in the residues. The comparison of the XRD data among the original PA6, Clay, and PA6/Clay(5%), and the black residues collected at various fractions of sample mass losses corresponding to the pictures shown in Fig. 8. The XRD data of the PA6 shows the two peaks corresponding to mainly to the α crystalline phase; that of the original Na-clay shows many peaks with the d-spacing of about 1.19 nm (at 2θ of about 7.44°). However, the PA6/Clay(5%) original sample shows a sharp peak at 2θ of about 21.4° corresponding to the γ crystalline phase. Such effects of the addition of clay to PA6 on the crystallinity were well documented in previous studies [21,22,23]. The data for the carbonaceous floccule residue collected at $W/W_0 = 0.90$ (10% loss), corresponding to the picture shown in Fig. 8, consists of a new peak at about $2\theta = 6.44°$, corresponding to the d-spacing of 1.37 nm, of all peaks of the clay except the peak at $2\theta = 19.8°$, and of the γ crystalline phase of PA6. With further sample mass loss (longer exposure to the external radiant flux), the XRD data of the collected black residues show the reduction in the γ crystalline phase of PA6 in the residues and any PA6 characteristic structures disappear from the residues collected after losing more than 38% of the sample mass loss. This observation is nearly consistent with that shown in Fig. 10 (the residues collected at more than 21% sample mass loss do not possess any degradation peak for PA6). The d-spacing of the clay in the black residues gradually decreases with the increase in sample mass loss such as from 1.37 nm at $W/W_0 = 0.10$ to 1.30 nm at $W/W_0 = 0.95$. Since the d-spacing of the original clay (without organic treatment) was 1.19 nm, it appears that some organic materials could be trapped in the space between the clay platelets. A new peak is observed at about 2θ of 26.5° for the black residue collected at $W/W_0 = 0.10$. This peak became broader for the residue collected at $W/W_0 = 0.21$ and spread to two peaks at 26.5 and 27.3° for the residue collected at $W/W_0 = 0.38$. The latter peak became more dominant than the former peak for the sample collected with further sample mass loss. These peaks (3.35 and 3.25 Å) are very close to that of the ordered graphite spacing of 3.354 Å [24]. The results shown in Fig. 10 indicate high thermal stability for the organic

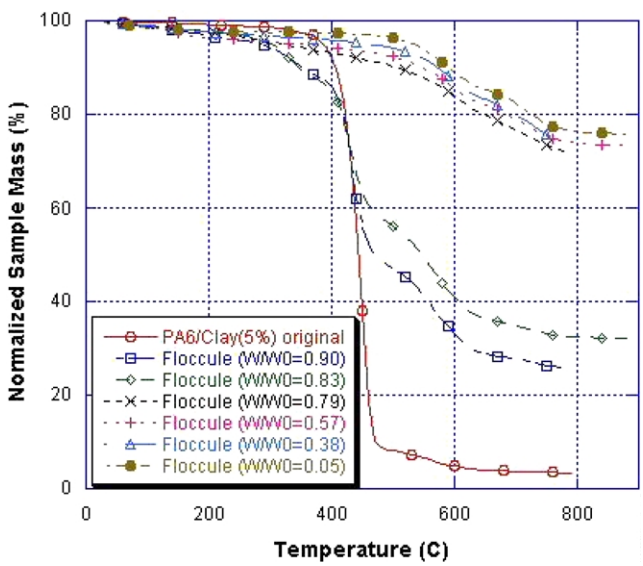

Fig. 9. TGA of carbonaceous floccules of PA6/Clay(5%), collected at various sample losses at external flux of 50 kW/m^2 in N_2 under air at heating rate of 10 °C/min.

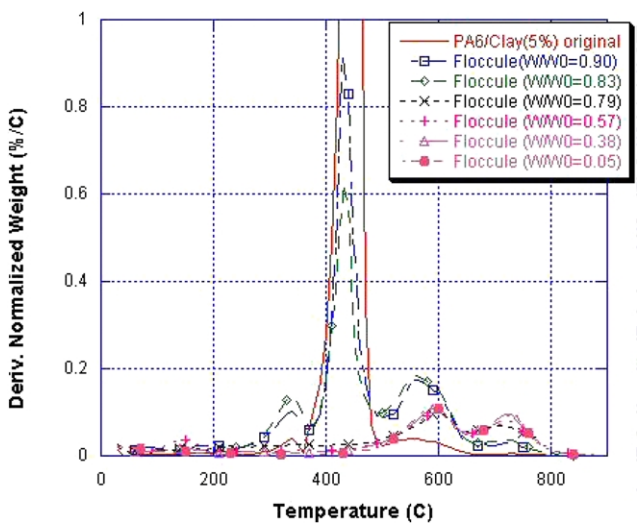

Fig. 10. DTG plot of carbonaceous floccules of PA6/Clay(5%) collected at various sample mass losses at external flux of 50 kW/m^2 in N_2.

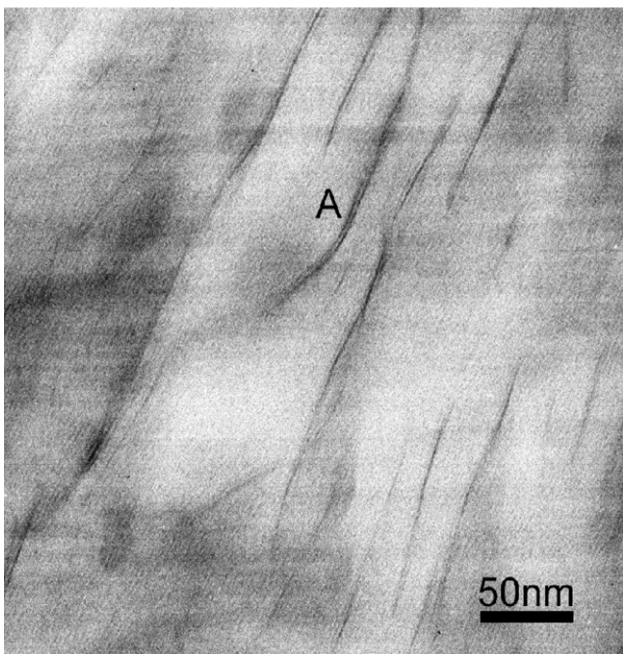

Fig. 11. TEM image of the original (injection molded) PA6/clay(5%) sample.

components in the carbonaceous floccule residues collected at higher sample mass losses ($\geq W/W_0 = 0.21$). These results indicate that the PA6/clay (5%) sample tends to form a small quantity of highly, thermally stable organic components possibly having a graphitic structure. It is speculated that such structure could be formed in the narrowly spaced clay platelets which were abundant in the black residues (clay contents close to 80% of mass fraction of the residue collected above $W/W_0 = 0.21$, as shown in Fig. 9).

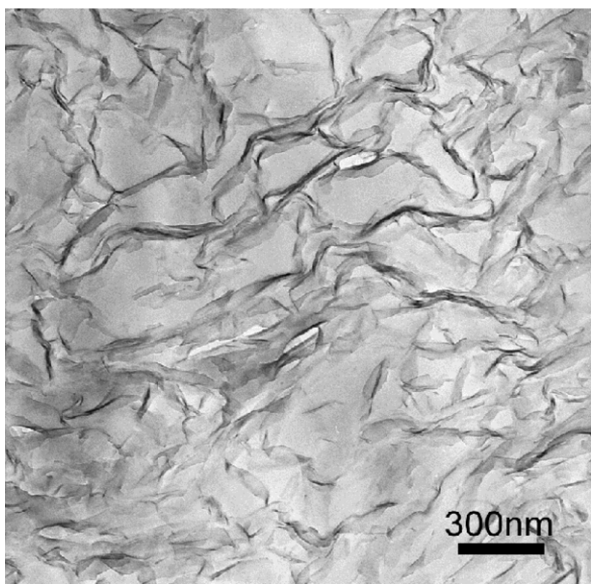

Fig. 12. TEM image of the carbonaceous floccule residue collected at 17% sample mass loss at 50 kW/m^2 in a nitrogen atmosphere.

4. Discussion

When the surface of a thermoplastic sample is heated by an external source, or by heat feedback from a flame, the temperature near the surface rapidly increases followed by reduction in viscosity of the molten sample near the surface. When the temperature of the PA6 sample becomes sufficiently high, degradation starts to generate pyrolysis products. The majority of products are monomer, cyclic oligomers plus small quantities of gaseous volatiles [25,26]. The degradation temperature of the PA6 sample is much higher than the boiling temperature of the monomer (136–138 °C) and is at least as high as some of the cyclic oligomers. Thus, the degradation products are superheated and readily nucleate, forming bubbles in the molten layer. The addition of clay particles could enhance heterogeneous nucleation and subsequent bubbling. The bubbles rapidly rise and expand to the sample surface if the surrounding polymer layer is a low viscosity melt. Rising bubbles create convective motion in the molten layer. One possible effect of bubbles on clay particles can be seen in Fig. 13. Nanometer sized bubbles (white regions representing little carbonization) can be seen in this figure. Clay platelets in the vicinity of these bubbles are deformed and pushed into a stacked structure apparently by the movement of the bubbles. Positions labeled ‘A’ are stacks close to the bubble, ‘B’ are isolated stacks, and ‘C’ are exfoliated clay platelets. A spacing of 1.6 nm to 2.4 nm was measured between the platelets in this stacked structure from the TEM

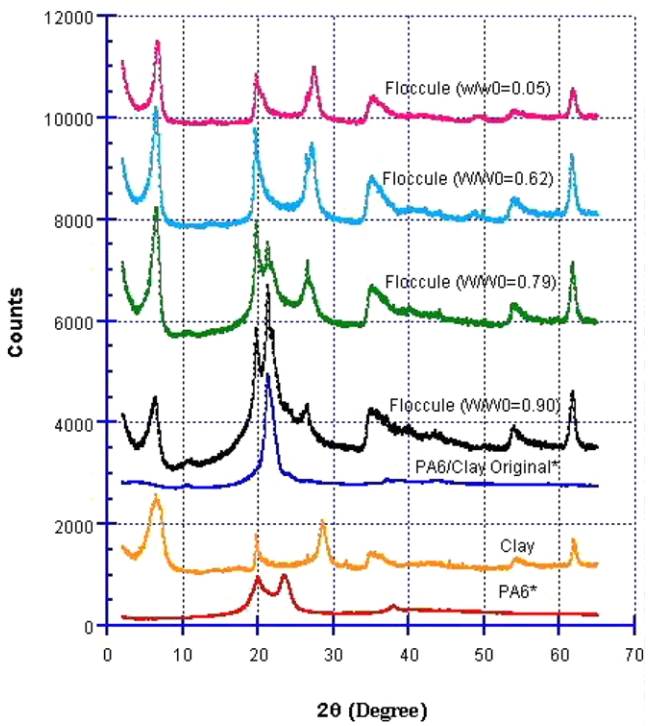

Fig. 13. XRD of PA6, Clay, PA6/Clay(5%), and carbonaceous floccules collected at various fractions of sample mass loss at 50 kW/m^2 in N_2. *PA6 and PA6/Clay original values reduced to 10% of measured values.

images. In the non-carbonized region (outside of the carbonaceous floccules) of the residue, there is also a significant amount of stacked clay platelets which is in contrast to the starting material which shows minimal stacked groups of clay platelets (as shown in Fig. 11) and the clay is completely exfoliated. The stacking of clay particles was also observed in the having high content of clay (as shown in Fig. 9) by the XRD data shown in Fig. 14. The extra spacing between the platelets might be occupied by thermally stable organic components with a graphitic nature such as carbonaceous char, as described in Section 3.

We would like to know how the initially well-dispersed clay particles in the sample tend to accumulate on the sample surface during burning/gasification to form protective floccules consisting of thermally stable organics (some of which could be carbonaceous char). One possible mechanism is due to recession of the polymer resin from the surface by pyrolysis leaving the clay particles behind. It is expected that at high temperature the amine grafted organic polymer layer will degrade from the clay particle surface [20] resulting in more hydrophilic and less compatible clay particles with resin. Thus, the hydrophilic clay particles might then tend to separate from the resin and aggregate into stacks, particularly under the influence of the bubbling polymer matrix. Although the density of the clay is 2.6 g/cm^3 [27] and it is heavier than PA6, the accumulated floccules filled with clay particles were porous and light enough for staying on the surface without sinking into the polymer melt layer. Another possible mechanism might be a transportation of clay particles pushed by numerous rising bubbles and the associated convection flow in the melt from the interior of the sample toward the sample surface. The migration of clay particles by diffusion or by surface tension forces to the sample surface tends to be much slower than the two above-described possible transport mechanisms and appear to be negligible. Numerous rising bubbles have another effect on the transport of clay particles. Bursting of the bubbles at the sample surface pushes any accumulated clay particles on the melt sample surface outward from the bursting area promoting agglomeration into the island-like floccules rather than the formation of a continuous net-like structure of a clay filled protective layer. This is in contrast to a net-like protective layer that has been observed in high molecular mass PMMA silica gel system [16].

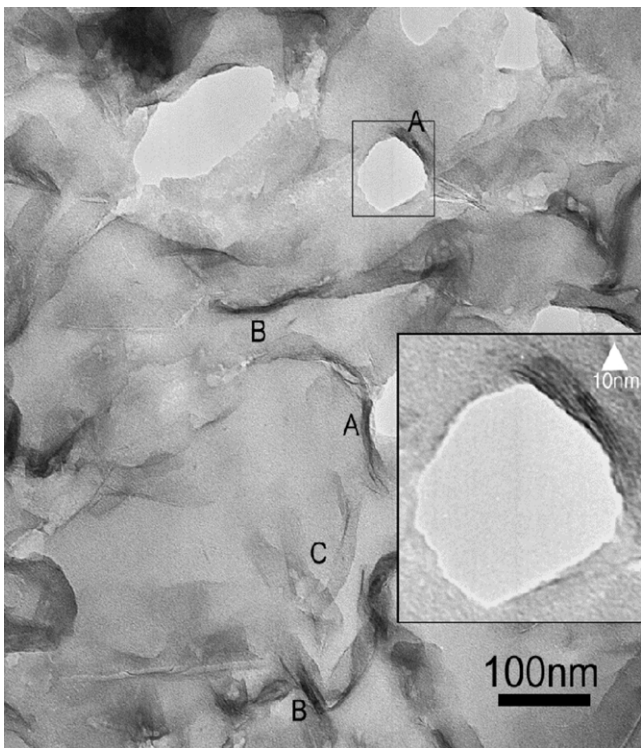

Fig. 14. TEM image of the white part (outside of carbonaceous floccule) of the residue colected when the PA6/Clay(5%) sample lost 17% of its mass at 50 kW/m^2 in N_2.

The amount and size of the protective floccules depend on (1) the initial content of clay in the polymer, (2) char forming characteristics of the polymer, (3) melt viscosity of the sample, and (4) the aspect ratio of the nanoscale additive. The PA6 sample forms little char (less than 1% of the initial sample mass). With 2% of clay content in PA6, many small, protective floccules are formed as shown in Figs. 6 and 7. With 5% of clay content in PA6, more and larger protective floccules are formed as shown in the same figures. However, the protective floccules did not cover the entire sample surface and vigorous bubbling was observed on the unprotected surface exposed to the external heat flux. The vigorous bubbling and the formation of the protective floccules could be due to the relatively low melt viscosity of the three samples, as shown in Fig. 2. The importance to the FR performance of suppressing the vigorous bubbling and forming solid-like sample behavior via a higher melt viscosity resin has been demonstrated with the PMMA/silica samples having two different molecular masses [16]. Covering the entire sample surface by clay particles plus thermally stable organics such as char is highly desirable in order to have effective FR performance of clay-polymer composites. The ideal structure of the protective surface layer (consisting of clay particles and char) is net-like and has sufficient physical strength not to be broken or disturbed by bubbling. The protective layer should remain intact over the entire burning period. Although the PA6/clay nanocomposite sample studied here formed such a protective layer covering a part of the sample surface, it was reported that the polystyrene/clay nanocomposite sample formed such a protective layer covering the entire sample surface [14]. This could be due to enhanced formation of char from PS by the addition of clay. However, several large cracks were observed in the residues of this particular PS/clay nanocomposite sample.

The formation of a net-like protective layer near the sample surface can be achieved by the use of a sample having high melt viscosity at high temperatures. High melt viscosity tends to suppress the convection motion induced by vigorous bubbling through the molten layer. Added

particles tend to be left to form (due to gradual consumption of polymer) a net-like layer near the sample surface. The required higher melt viscosity could be achieved by the use of a higher molecular mass polymer, by having particles with a larger surface area (or a large aspect ratio) such as clay [27,28], and by having a high content of the additive particles. Particles with a larger surface area or a large aspect ratio have another advantage since they tend to form a net-like structure compared to particles with a small surface area [16] or a small aspect ratio [29]. One such example of a high aspect ratio particle is the carbon nanotube and polypropylene/multi-walled carbon nanotube (MWNT) samples which formed a protective layer covering the entire sample surface without any cracks [30]. With the addition of MWNT of only mass fraction of 1%, a significant reduction in heat release rate of polypropylene was reported without using any surfactant. Another approach could be the use of specific organic treatments on the nano-particle surface to form a significant amount of crosslinkages with the polymer at high temperatures. This would tend to enhance char formation and would aide in forming a net-like layer.

5. Conclusion

The PA6/clay nanocomposite samples (clay contents of 2 and 5% by mass with 8 mm thickness) significantly reduce the peak heat release rate of the PA6 sample. This reduction in the peak heat release rate is achieved by the formation of protective floccules on the sample surface which shield the PA6 from the external thermal radiation and heat feedback from the flame, thus acting as a thermal insulation layer. The analysis of the protective floccules, collected at various sample mass losses, shows up to 80% by mass of the floccules consisting of clay particles. The remaining 20% consists of thermally stable organic components with possible graphitic structure. Furthermore, clay particles are stacked and the d-spacing of the clay platelets is in the range of 1.3–1.4 nm as compared to well-exfoliated original sample. The accumulation of the initially well-dispersed clay particles in the sample on the burning/gasifying sample surface are due to two possible mechanisms. One is recession of the polymer resin from the surface by pyrolysis with de-wetted clay particles left behind. Clay particles tend to aggregate and stack against each other after the degradation of the organic treatment on the clay surface making them more hydrophilic and less compatible with the resin. Another mechanism is the transportation of clay particles pushed by numerous rising bubbles of degradation products and the associated convection flow in the melt from the interior of the sample toward the sample surface. Numerous rising bubbles have another effect on the transport of clay particles. Bursting of the bubbles at the sample surface pushes the accumulated clay particles outward from the bursting area and forms the island-like floccules instead of forming a continuous net-like structure of a clay filled protective layer. Therefore, both PA6/clay nanocomposite samples did not produce sufficient amounts of protective floccules to cover the entire sample surface and vigorous bubbling was observed over the sample surface which was not covered by the protective floccules.

Acknowledgements

This study is funded by the FAA Technical Center under the grant number of 02-G-022 to the University of Maryland and DTFA03-99-X-90009 to NIST. The authors thank UBE Industries Ltd for kindly providing the PA6 and PA6/clay samples used in this study.

References

[1] Kojima Y, Usuki A, Kawasumi M, Okada A, Fukushima Y, Kurauchi T, Kamigaito OJ. Mater Res 1993;8:1185–9.
[2] Giannelis EP. Adv Mater 1996;8:29–35.
[3] Wang Z, Pinnavaia TJ. Chem Mater 1998;10:1820–6.
[4] Zanetti M, Camino G, Thomann R, Mülhaupt R. Polymer 2001;42:4501–7.
[5] Pluta M, Galeski A, Alexandre M, Paul M-A, Dubois P. J Appl Polym Sci 2002;86:1497–506.
[6] Ray SS, Okamoto K, Okamoto M. Macromolcules 2003;36:2355–67.
[7] Gilman JW, Kashiwagi T. SAMPE J 1997;33:40–6.
[8] Gilman JW. Appl Clay Sci 1999;15:31–49.
[9] Gilma JW, Jackson CL, Morgan AB, Harris Jr R, Manias E, Giannelis EP, Wuthenow M, Hilton D, Phillips SH. Chem Mater 2000;12:1866–73.
[10] Beyer G. Fire Mater 2001;25:193–7.
[11] Zanetti M, Camino G, Mülhaupt R. Polym Degrad Stab 2001;74:413–7.
[12] Zhu J, Uhl FM, Morgan AB, Wilkie CA. Chem Mater 2001;13:4649–54.
[13] Alexandre M, Beyer G, Henrist C, Cloots R, Rulmont A, Jerome R, Dubois P. Macromol Rapid Commun 2001;22:943–6.
[14] Zhu J, Start P, Mauritz A, Wilkie CA. Polym Degrad Stab 2002;77:253–8.
[15] Morgan AB, Harris Jr RH, Kashiwagi T, Chyall LJ, Gilman JW. Fire Mater 2002;26:247–53.
[16] Kashiwagi T, Shields JR, Harris Jr RH, Davis RD. J Appl Polym Sci 2003;87:1541–53.
[17] Krishnamoorti R, Giannelis EP. Macromolecules 1997;30:4–97. see also page 4102.
[18] Khanna YP, Han PK, Day ED. Polym Engng Sci 1996;36:1745–54.
[19] Austin PJ, Buch RR, Kashiwagi T. Fire Mater 1998;22:221–37.
[20] Davis RD, Gilman JW, VanderHart DL. Polym Degrad Stab 2003;79:111–21.
[21] VanderHart DL, Asano A, Gilman JW. Chem Mater 2001;13:3781–95.
[22] Lincoln DM, Vaia RA, Wang ZG, Hsiao BS. Polymer 2001;42:1621–31.
[23] Fornes TD, Paul DR. Polymer 2003;44:3945–61.
[24] Reznik D, Olk CH, Neumann DA, Copley JRD. Phys Rev 1995;52:116–24.
[25] Levchik SV, Costa L, Camino G. Polym Degrad Stab 1992;36:229–37.

[26] Pagilagan RU. In: Kohan MI, editor. Nylon plastics handbook. Cincinnati, OH: Hanser/Gardner; 1995. Chapter 3.
[27] Krishnamoorti R, Giannelis EP. Macromolecules 1997;30:4097–102.
[28] Pőtschke P, Fornes TD, Paul DR. Polymer 2002;43:3247–55.
[29] Kashiwagi T, Morgan AB, Antounucci JM, VanLandingham MR, Harris Jr RH, Awad WH, Shields JR. J Appl Polym Sci 2003;89: 2072–8.
[30] Kashiwagi T, Grulke E, Hilding J, Harris Jr RH, Awad WH. J Macromol Rapid Commun 2002;23:761–5.